

Predicting air temperature simultaneously for multiple locations in an urban environment: A bottom up approach



Shai Kaplan^{*}, Aviva Peeters, Evyatar Erell

Desert Architecture and Urban Planning Unit, Swiss Institute for Dryland Environmental and Energy Research, Jacob Blaustein Institutes for Desert Research, Ben-Gurion University of the Negev, Israel

ARTICLE INFO

Article history:

Received 5 March 2016

Received in revised form

10 September 2016

Accepted 11 September 2016

Keywords:

Computer modelling

Urban heat island

Urban planning

Spatial variability

GIS

ABSTRACT

Cities are characterized by high heterogeneity that results in varied microclimate effects. The current study introduces a new bottom-up approach linking the urban Canyon Air Temperature (CAT) model with spatially distributed inputs extracted from a GIS data-base and remote sensing products to predict intra-urban temperature variability simultaneously for multiple locations in an urban environment. To provide proof of concept, the model was applied for the city of Bat-Yam, Israel. Simulation shows a maximum nighttime urban heat island (UHI) intensity of 2–2.25 °C, relative to a rural reference point, during both summer and winter, with significant spatial variability related to the height-to-width ratio of urban street canyons and to the surface land cover. The CAT simulation also highlighted the important influence of the local wind regime on the development and persistence of the nocturnal UHI. We conclude that linking CAT to a GIS data-base supports simulations at the city scale that reflect the local intra-urban variability. The model can be used to investigate both macro and micro scale spatio-temporal characteristics of the UHI in various urban development scenarios, which may be applied to generate appropriate geographically-explicit mitigation and adaptation measures.

© 2016 Elsevier Ltd. All rights reserved.

1. Introduction

The link between cities and climate and its impact on human comfort and building energy consumption is often evaluated using sophisticated model simulations. These models may rely on weather data obtained from the nearest station outside the city or at the nearest airport. However, the data represent historical climate rather than current or future conditions urban dwellers and infrastructure will be exposed to. Furthermore, cities are characterized by high heterogeneity that results in substantial intra-urban variations of the microclimate. In other words, the weather at any given location within the urban area may differ in a meaningful way from that of the reference weather station.

The rapid urbanization of the past 50 years has changed the physical urban environment, creating a more heterogeneous landscape. Cities are known to be warmer than their rural surroundings due to different thermal, radiative, moisture and aerodynamics characteristics of the built environment (Howard, 1820; Oke, 1973, 1987), a phenomenon referred to as the urban heat

island (UHI). However, many studies show that the UHI is not uniform in time or space: It is typically greatest on clear, windless nights (Oke, 1981), and land cover heterogeneity has a significant spatial effect on air temperature (Erell & Williamson, 2007; Georgescu, Moustouli, Mahalov, & Dudhia, 2012; Lookingbill, 2003; Loridan & Grimmond, 2012; Oke, 1981, 1982; Pielke, 2001; Weaver & Avissar, 2001). A comprehensive review of UHI research can be found in Arnfield (2003). The UHI does not only impact the physical environment but further exacerbates thermal stress through changing the energy balance both between the surface and the atmosphere and between the human body and the atmosphere.

Thermal stress has been associated with heat related vulnerability (illnesses and death) (Guo et al., 2014) and epidemiological studies have described a substantial increase in morbidity and mortality in conjunction with heat episodes (Basu & Samet, 2002), of which the 2003 heat wave in Europe is a well-known example (Robine et al., 2008). Rosenthal, Kinney, and Metzger (2014) demonstrated that, crucially, excess mortality was strongly related to the physical properties of neighborhoods, so mitigating the effects of future heat events requires a means of assessing which neighborhoods are most likely to suffer from overheating.

^{*} Corresponding author.

E-mail address: kaplans@bgu.ac.il (S. Kaplan).

Although air temperature is but one factor contributing to thermal stress, the evidence from numerous epidemiological studies indicates that it is of sufficient importance for detailed study even in the absence of contemporaneous data on other factors such as the radiant exchange and humidity.

Numerous studies (Merbitz, Buttstädt, Michael, Dott, & Schneider, 2012; Rotem-Mindali, Michael, Helman, & Lensky, 2015; Saaroni, Ben-Dor, Bitan, & Potchter, 2000) have indicated the importance of urban characteristics, such as land-use, building density, vegetation or materials on the spatial pattern and complexity of the UHI. For example, Saaroni et al. (2000) found both positive and negative pockets of UHI within Tel-Aviv city center. Chow and Roth (2006) found intra-urban UHI differences >1 °C in Singapore and attributed it to enhanced anthropogenic heat, green spaces and distance to the water front. Similar findings were reported for Hong-Kong by Giridharan, Ganesan, and Lau (2004; 2005). Hart and Sailor (2009) reported UHI intensity differences of up to 10 °C within Portland between areas with high canopy coverage and surrounding urban regions. Furthermore, they found freeways and major roads experience UHI of up to 5 °C while both the downtown and suburban areas experience temperature anomalies of up to 2 °C.

Recent studies adopt a more nuanced approach, so that the rural-urban dichotomy is replaced by a continuum of Local Climate Zones (LCZs), classified according to built form, materials and land cover (Stewart & Oke, 2012). Nevertheless, most mesoscale climate models cannot account fully for this heterogeneity, resulting in a contrast between the micro-scale, where the land cover and 3D characteristics impact climate at street level, and the spatial scale at which these models operate, which is typically a grid resolution of 500 m or more.

To obtain detailed microscale air temperature maps, researchers have used high density direct point measurements, remote sensing, or numerical modelling. Direct measurements are labor intensive, require expensive instrumentation and high spatial density, as well as a substantial logistical outlay to provide data over extended periods. Regression and geo-statistical models produced from direct measurements are used to provide interpolated data for locations where no physical measurements were recorded, but these are often site-specific and still require a fairly dense measurement network (Ivajnsič, Kaligarić, & Žiberna, 2014). Remote sensing does not measure canopy layer air temperature directly, but rather 'skin' (surface) temperature. Several studies have demonstrated good correlation between the radiant temperature and canopy level air temperature (Kloog, Chudnovsky, Koutrakis, & Schwartz, 2012, 2014; Pelta, Chudnovsky, & Schwartz, 2016), and the technique has been applied in research on the effect of heat waves on mortality (Laaidi et al., 2012). However, the linkage between surface and air temperature is extremely complex and the models may not always predict air temperature from remotely sensed skin temperature accurately. Moreover, the temporal resolution of satellites may not be sufficient to produce the hourly or daily time series needed to monitor and model the nocturnal UHI (Yang, Endreny, & Nowak, 2013). Numerical models based on fluid dynamics such as ENVI-met (Bruse & Fleer, 1998) have also been applied in numerous studies, but they are best suited to scenario testing in short time-scales and limited spatial extent. They require very detailed input and substantial computational resources, so they are still limited to research rather than planning applications.

Land surface models (LSM) such as the Noah LSM embedded within the Weather Research and Forecasting model (WRF) and the Town Energy Balance model (TEB) (Hamdi & Masson, 2008; Masson, 2000) overcome some of the limitations mentioned above, and have been applied in many major metropolitan regions in different climate zones (Georgescu et al., 2012; Grimmond, 2007;

Oleson, Bonan, Feddema, Vertenstein, & Grimmond, 2008). LSMs use thermo-dynamics to estimate the land surface energy fluxes and their partitioning to latent and sensible heat. However, these models are computationally intensive and represent the urban surface in a parameterized fashion, including the urban canopy state variables such as albedo and thermal properties of the built environment and its 3D representation; i.e. they do not represent buildings explicitly or their complex interactions such as long- and short-wave radiation interactions and urban canyon wind channeling effects. Moreover, because spatially distributed boundary and initial conditions are not available for most urban areas (e.g. radiation components), LSMs use mesoscale climate models' output as input and apply a top-down approach in which heat flux is determined by the difference between the model's vertical layers. These requirements limit the model grid size (>500 m), impairing their ability to capture the high heterogeneity of land cover and 3D parameters over small distances that characterizes some built environments.

One such model, PASATH, (Spatial Air Temperature and Humidity) is a physically based analytical model that can provide spatially and temporally detailed microclimate maps (Yang et al., 2013). Similar to WRF, PASATH does not provide a full spectrum of height-to-width ratio, but rather a parameterization scheme for 4 urban canyon types: open space, low-, medium-, and high-intensity development. While this simplification allows the model to be less data-driven and less computationally intensive, it limits its capability to represent the high heterogeneity of some urban areas. Furthermore, the PASATH model uses additional sub-models that require expert knowledge as well as elevation data, and does not include an atmospheric stability correction. This limits its accuracy in calculating aerodynamic resistance.

Over the last decade, GIS technology and 3D digital data have become more widely accessible. These databases may be used to produce temperature maps, usually grid-based maps in varying resolutions, which represent the spatial variation in temperature across the city (Jusuf & Hien, 2009). Ren, Ng, and Katzschner (2011) provided a review of urban climate map studies and demonstrated the need to incorporate climatic aspects into the urban planning, development and decision making processes. They pointed out the advantages of using a GIS-based platform for analyzing and visualizing the urban thermal environments, and concluded that future research should focus on spatial analysis and creating a simplified method to provide spatially explicit climate information for urban outdoor areas. Recently, Kastendeuch and Najjar (2015) developed the LASER/F urban canopy model designed to work with high resolution 3D city geometry from a GIS database. However, the model requires much processing power and time and cannot be used at a city scale. Furthermore, the simulation uses a top-down approach in which the boundary conditions are imposed at the top of each urban canopy box.

The current study introduces a new bottom-up approach in which the point-based urban Canyon Air Temperature (CAT) model developed by Erell and Williamson (2006) is adapted to modelling at a larger spatial scale by linking drawing inputs from a GIS database and remote sensing products to predict air temperature simultaneously for multiple locations in an urban environment. The number of urban locations that can be modeled is not limited and therefore a detailed and more accurate representation of the spatial variations of the urban micro-climate can be generated. CAT offers a mechanism for capturing micro-climate variations resulting from local surface characteristics and canyon geometry. Utilizing GIS to create a detailed spatial urban canyon morphology database allows us to run detailed high resolution CAT simulations that take into account the 3D characteristics and heterogeneity of the urban landscape, and evaluate the spatio-temporal variability of micro-

climate. Model outputs may be applied to the study of pedestrian thermal comfort, to generate urbanized inputs for building energy modelling and to assist in the development of future urban plans.

The objectives of the research reported here are: (a) to develop a methodology for extracting 3D urban characteristics from GIS and remote sensing images in a format suitable for microclimate modelling, and (b) to provide proof-of-concept for a spatio-temporal model that can simultaneously predict air temperature for numerous locations in an urban environment and represent the spatial variability of urban air temperature in a variety of weather conditions.

2. Materials and methods

2.1. The CAT model

The Canyon Air Temperature (CAT) model (Erell & Williamson, 2006) was designed to predict site-specific micro-meteorological conditions in an urban street canyon for extended periods, based on data from a reference station exposed to the same meso-scale weather. The required inputs for the CAT model are: a geometric description of the street canyon and the nearby standard meteorological station; the land cover, specifically the proportions of vegetation and water around each site; and time-series of the meteorological parameters measured at the weather stations, typically at hourly intervals. The latter are used to describe and characterize the constantly evolving meso-scale weather. A representative meso-scale base temperature is then calculated based on site-specific modifications to air temperature resulting from the surface energy balance at the reference site. The base temperature is in turn used to calculate the evolution of air temperature at the urban canyon based on a similar energy balance calculation reflecting the specific properties of this site. The procedure may be carried out for all weather conditions and for time periods ranging from a single month to a year or more.

CAT incorporates several parameterization schemes, based on field studies reported by other researchers, which were subsequently tested within the framework of the current model. In addition to expressions for estimating the effect of wind speed on the convective surface heat transfer coefficient and the effect of moisture availability on sensible heat flux, CAT also uses an empirical correlation between the sol-air temperature of an exposed reference surface and a coefficient of mixing between the urban canopy and the mixed layer above roof height, which was developed specifically for this purpose. The latter is estimated by a simplified indicator based on the difference between air temperature at screen height and the surface temperature of the ground.

The CAT model was calibrated and tested using experimental data obtained in an extended monitoring program carried out in Adelaide, South Australia (Erell & Williamson, 2006). Comparison of measured and predicted canyon air temperature showed good agreement with a mean square error (MSE) < 1.5 °C and systematic MSE < 0.2. These results, along with analysis of the relationship to several environmental indicators, support the claim that there are no major unexplained factors missing from the model.

Further validation was carried out using data obtained from an independent microclimate experiment carried out in Gothenburg, Sweden (Erell, Eliasson, Grimmond, Offerle, & Williamson, 2009, 2010). This version of CAT employs a parametric scheme to estimate moisture availability that is affected by advection from upwind source areas identified by wind direction and which also varies with atmospheric stability. Estimates of the variability of moisture due to advection from vegetation or bodies of water take into account direction-dependent upwind surface cover and the effect of atmospheric stability on the spatial extent of the source

area. The use of wedge-shaped polygons is an essential part of the methodology, which simplifies calculation. Unlike conventional weather models, which solve a complete set of equations governing the transfer of energy, mass and momentum from each grid cell to all adjacent ones, the method illustrated here adopts a simplified source-area model that assigns a wedge-shaped source area upwind of each grid point that is updated at each time step. The size of the source area is estimated based on Schmid and Oke (1990), with values for advection of moisture parameterized following Grimmond and Oke (2002). Similar to the Adelaide study, the Williamson degree of confirmation (Williamson, 1995) was in the range 0.3–0.5, indicating a substantial improvement over the use of raw data from the weather station. The model is thus considered capable of reproducing the street canyon temperature evolution and the nocturnal UHI for various climatic conditions and physical surroundings.

2.2. Study area

The study focuses on the city of Bat-Yam, Israel (Fig. 1). Bat-Yam is a commuter community south of Tel Aviv, in the core of Israel's coastal metropolitan area. It covers an area of 8.28 km² and has a total population of about 160,000. The city has a Mediterranean climate (Köppen Csa) with average annual precipitation of about 500 mm and mean daily temperature of 25.3 °C in summer (July) and 12.2 °C in winter (January) (Bitan & Rubin, 1994). The selection of Bat-Yam was due to an ongoing project for developing a water sensitive city and incorporating vegetation along storm-water runoff pathways in existing urban fabric, with the additional aim of improving the microclimate.

2.3. Input data

Organization of input data was based on a geodatabase schema that allows linking geographical datasets spatially in order to support overlay analysis. The geodatabase also supports topological rules which maintain the integrity of the data and assist in locating errors. The spatial projection was defined as the Israel TM Grid. Input variables for the CAT model include publicly available climate data from meteorological stations in TMY format, 3D characteristics of the city (i.e. the urban street canyons), and the proportion of vegetation and water in the source areas for moisture.

To derive these variables, the following datasets were obtained for the study area:

1. Two GIS vector datasets (source: Israel National Mapping Agency) - one of street center-lines and the other of building footprints, represented as polygons. Building data included base elevation and building heights. These data were used to calculate average building height and street width.
2. Remotely-sensed data: To map land cover and extract the location and fractions of vegetation and water bodies required for simulation of moisture availability, freely available Google Earth images were combined with WorldView-2 (WV2) images acquired on June 27, 2012 (Fig. 2). The WV2 data has 2m spatial resolution with 8 bands - Coastal (400–450 nm), Blue (450–510 nm), Green (510–580 nm), Yellow (585–625 nm), Red (630–690 nm), Red Edge (705–745 nm), Near-IR1 (NIR1; 770–895 nm), and Near-IR2 (NIR2; 860–1040 nm).
3. Meteorological data: A TMY file for Bet Dagan, the nearest Israel Meteorological Service weather station with a full and detailed data set, was used to provide reference conditions. The station, about 7 km from the center of Bat Yam, represents climate conditions in the central part of Israel's coastal plain.

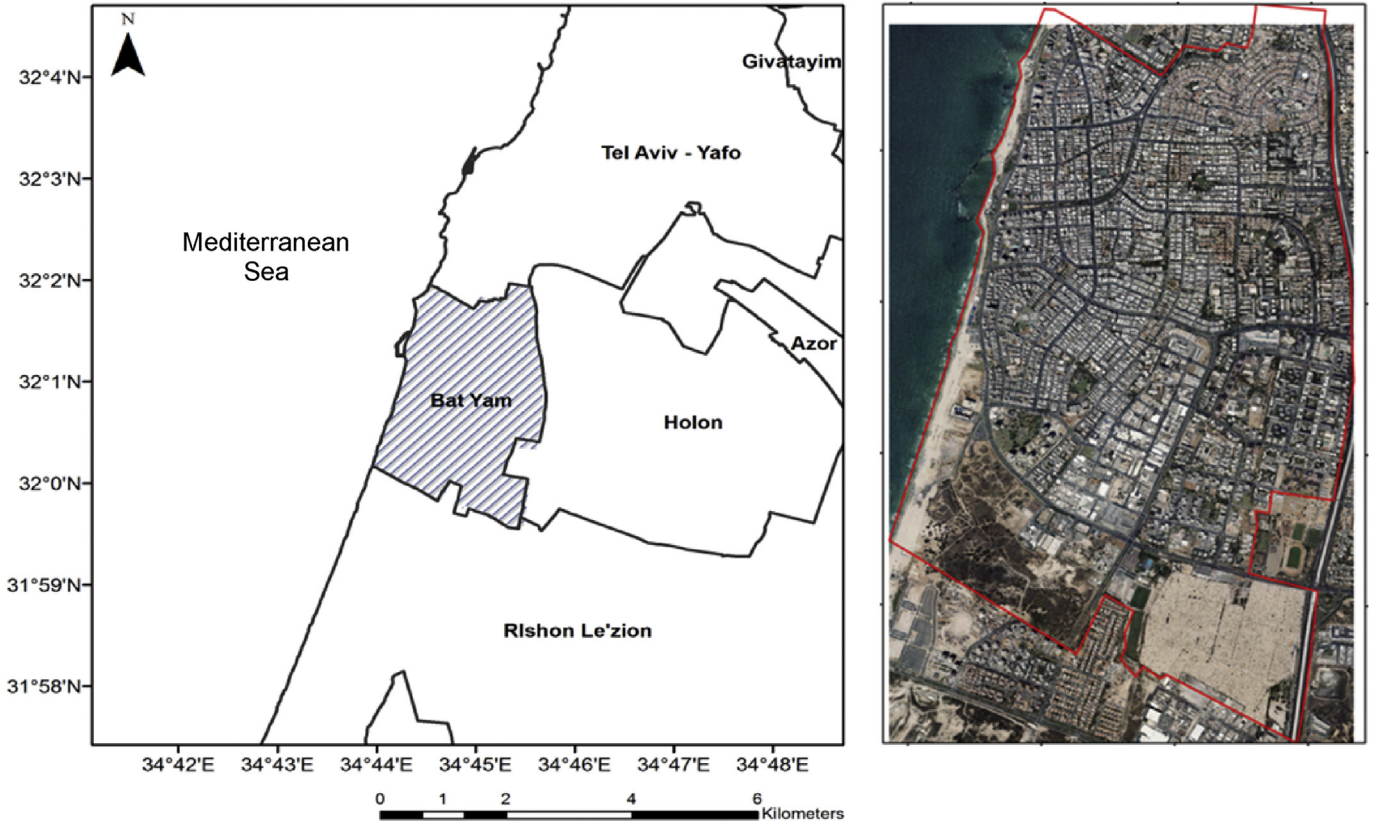


Fig. 1. Study area: location and aerial view of the city of Bat-Yam.

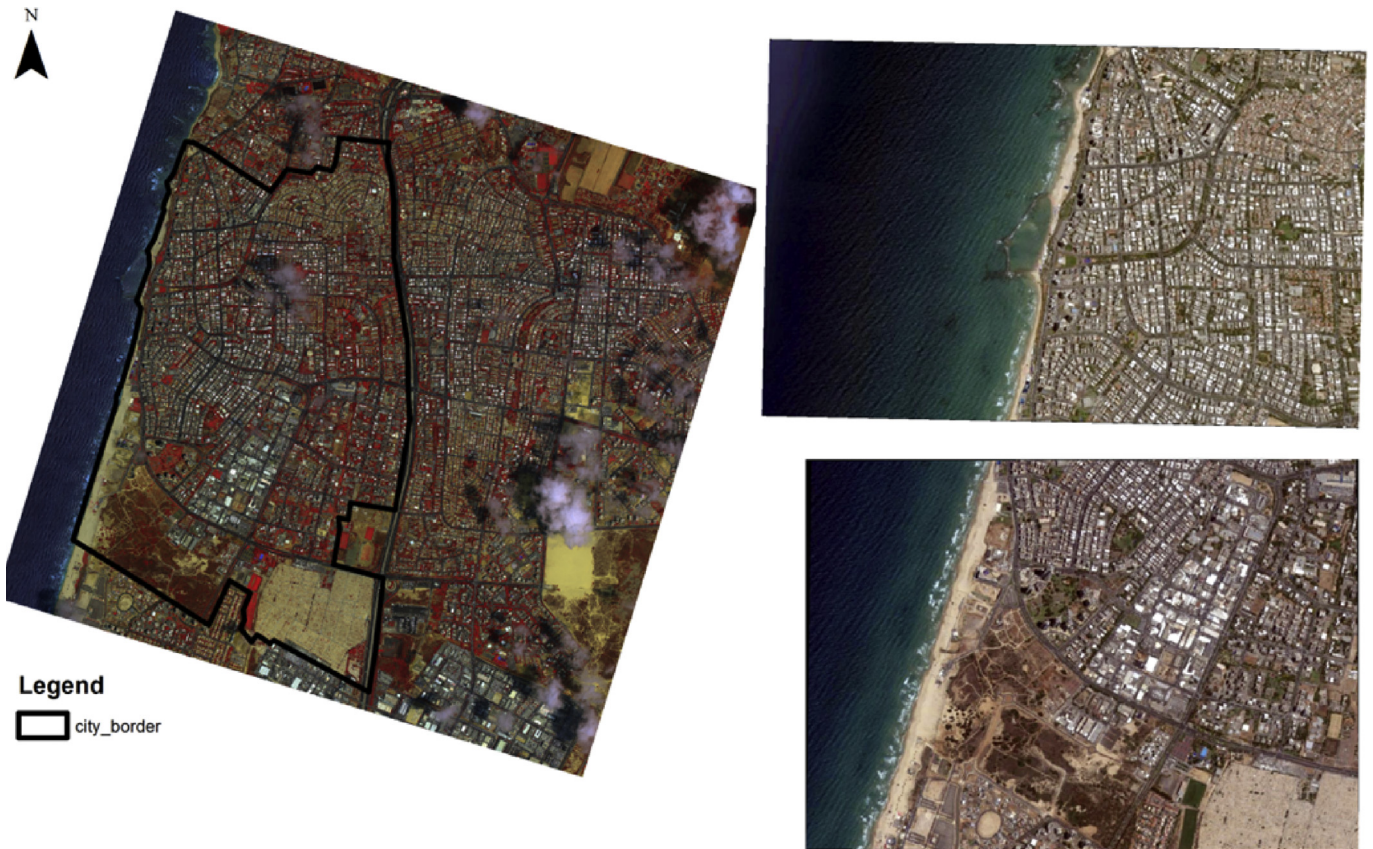


Fig. 2. Images used to extract land cover. Left: WorldView-2 image shown as false colors composites (R = NIR2, G = Red, B = Green). Right: The two Google Earth images used in the study. (For interpretation of the references to colour in this figure legend, the reader is referred to the web version of this article.)

2.4. Preparation of the urban data-base for the CAT simulations

Using data from these sources, two approaches were evaluated for assembling an input file suitable for processing in CAT: simulation of each individual street segment, in which the mid-point of every street vector was defined as a simulation point; and a grid approach, in which grid cells were populated with the average 3D characteristics of the streets within the cell boundaries. Exploratory data analysis revealed several limitations of the point-based approach, which are the result of the process through which the GIS data-base was compiled.

- First, what appeared through visual inspection of the city map and satellite image to be continuous streets were in fact sometimes coded as multiple segments. Secondly, the direction of digitization was inconsistent. For example: north-south streets were sometimes described as being south-north, giving a different value for the azimuth. Finally, streets with traffic islands and separator strips were sometimes coded as adjacent but separate segments. These 'technical' difficulties may be specific to the data-base used in this study, but are in all likelihood typical of many other such GIS files.

- Second, point-based spatial information is less effective as a visualization tool that planners, developers and decision makers can use.

Thus, a grid-cell approach was adopted. Following Mizuno, Nakamura, Murakami, and Yamamoto (1990) who found that the effect of local microclimate ranged from 50 to 200 m, and because CAT is a 2.5-dimensional model designed to work for an urban canyon at the street scale, a 150 m grid cell size was used. The drawback of the grid approach lies in the fact that each cell must first be classified as being either built-up or vegetated. The former type is represented by its averaged street canyon parameters, not accounting for some of the smaller scale features. The second type is represented by CAT as open space. Although the grid size specified was fairly small, some cells were nevertheless of a hybrid nature and consisted partly of streets and partly of open space.

The data were exported to an Excel spreadsheet and reorganized to remove unnecessary columns. To link them to the CAT model, a FORTRAN code was written that converts the data from the GIS format (where attributes for each point are specified in a line) to an input format readable by CAT (attributes arranged in a column).

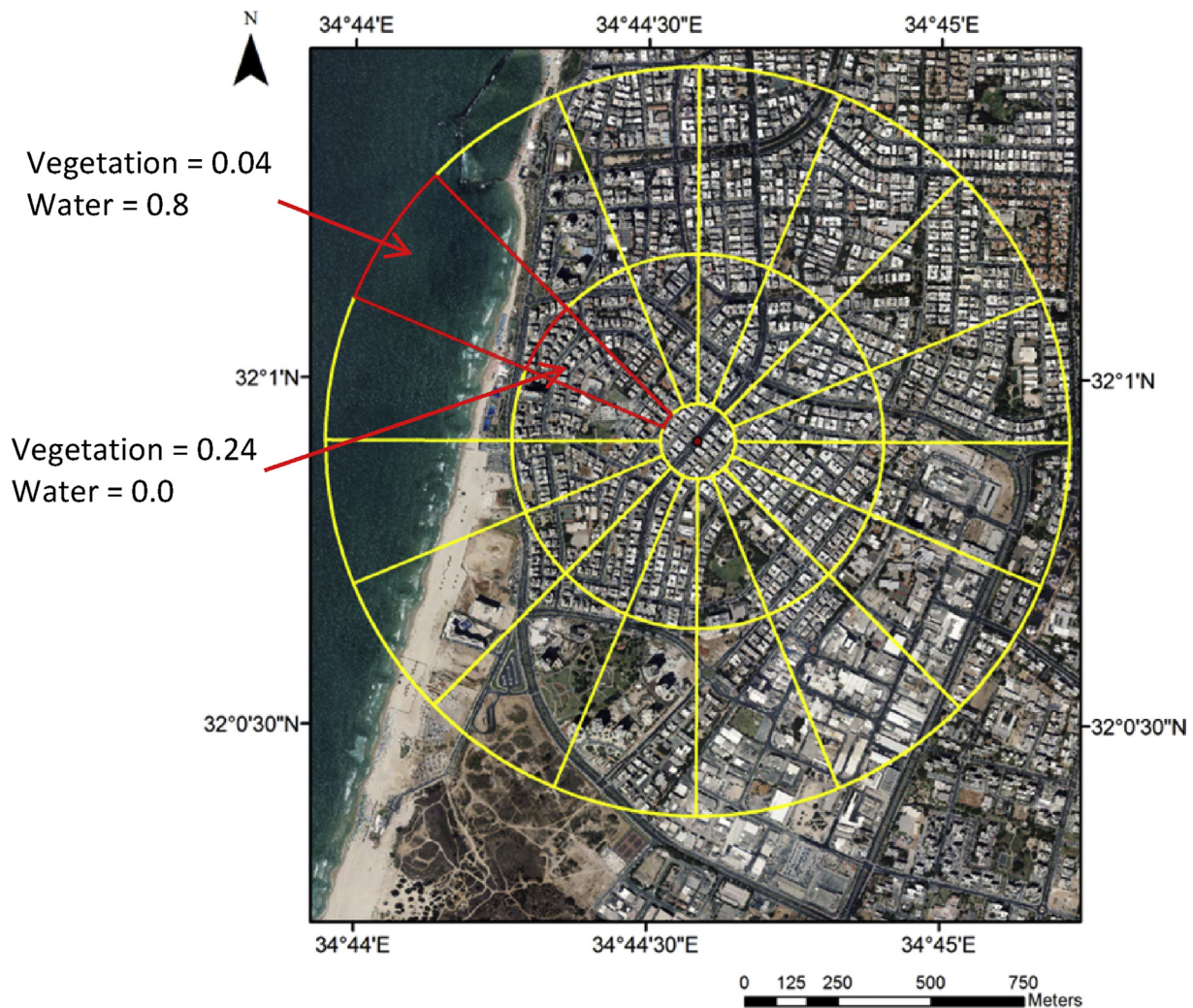


Fig. 3. Illustration of the method used to generate the wedges developed for extracting land surface cover in source areas for moisture at each grid point. Vegetation and water fractions for each sector are estimated from the database and used by CAT to parameterize moisture availability according to wind direction.

The method developed consists of the following steps:

2.4.1. Classifying vegetation and water land-cover

Vegetation and water mapping is required to calculate and account for local and advected moisture at a given point in time and space. Using the maximum likelihood classifier in ArcGIS 10.3 software package (ESRI, 1984) a Google Earth image of the pilot study area of Bat-Yam, Israel (Figs. 1 and 2) was classified. The maximum likelihood classifier is a non-supervised classifier (i.e. – the user does not select samples to represent land cover types), so initial classification was done by predefining the number of classes to 50. At the second stage, vector information of buildings and roads was incorporated to merge the initial 50 classes into 5 land cover types: buildings, open soil, impervious surfaces (roads, parking lots etc.), vegetation, and water.

As can be seen from Fig. 1, one limitation of using satellite images in urban areas is that shadows cast by buildings or vegetation hinder identification of the underlying surface cover. One option of addressing this limitation is to use a kernel window to incorporate shadows into their adjacent land cover using a statistical filter (e.g. 3×3 majority). In our case however, shadows accounted for less than 1% of the land cover, so the shaded area was ignored in the calculations. In cities with a higher shadow fraction, images taken as close as possible to the zenith may be used to minimize the shadowed areas where it may be very difficult to deduce the actual surface cover.

Another limitation of using Google Earth images is their limited spectral resolution, i.e. – only 3 bands in the visible range. This is especially important for vegetation because its most distinct spectral feature is its high reflectance in the near infrared (NIR) wavelengths. Thus, to enhance and improve vegetation mapping, the Normalized Difference Vegetation Index (NDVI) was calculated using the red and NIR bands of WV2:

$$\frac{(NIR2 - Red)}{(NIR2 + Red)}$$

The NDVI has been shown to have high correlation with plant biomass, leaf chlorophyll levels, leaf area index values and photosynthetically active radiation absorbed by the canopy; thus it is a measure of vegetation greenness/health (Lillesand, Kiefer, & Chipman, 2007). A threshold of $NDVI > 0.17$ was used to classify green vegetation pixels. The final land cover map was generated by overlaying the pixels identified as vegetation by WV2 NDVI on the

Google Earth image classification.

To systematically extract the percentage of vegetation and water around each point, taking into account the effect of orientation, we developed an automated GIS tool that constructs radial polygons around points based on defined azimuths and distances. Following CAT input requirements, the tool builds 32 wedges around a circle of 100 m radius surrounding each input point at distances of 500 and 1000 m (Fig. 3).

Using the Zonal Statistics method in ArcGIS (ESRI, 1984), the percentage of land cover (i.e. vegetation and water) in each wedge was calculated and assigned to each point. Zonal functions operate by analyzing the values of a group of cells in a raster based on a zone (area) defined by an overlaying dataset. The zones can be either polygons or groups of cells within another raster dataset (Lloyd, 2010). In the current study, the zones are defined by the output wedges. It is important to note that we used a single image to represent vegetation cover. In many cities urban vegetation is irrigated; thus it maintains its greenness regardless of climate. However, some vegetation, especially in open spaces and natural vegetation along the urban edges may be seasonal. In addition, evapotranspiration changes according to water availability and atmospheric demand, so vegetation impact might need to be adjusted seasonally.

2.4.2. Extracting 3D street variables

One of the most important characteristics which determine UHI intensity is the street geometry – i.e., height-to-width ratio and orientation (Oke, 1981, 1982). ArcGIS 10.3 was used to estimate the street width and mean buildings height along each street. Data were then averaged in a 150×150 m grid (see section 2.4).

2.4.2.1. Street width. Using the buildings footprint layer as input, a 1 m resolution raster of the shortest distance between each two buildings was generated. Following, a buffer of 2 m along the road centerline layer was created. To estimate the street width we used the Zonal Statistics method in ArcGIS (ESRI, 1984), where the centerline buffers were defined as zones, and the input raster was the shortest distance raster. The result of this procedure is that each street is represented by the minimum distance between buildings along its sides. Because the minimum distance represents only one side of the street (i.e. the closest building to the street center), the final width was determined by multiplying the value for each street by a factor of 2.

Table 1

CAT input describing the urban canyon site.

Characteristics of urban canyon site	Source	Value used/Range
Mean surface albedo ground	Remote sensing (Liang, 2000)	0.08–0.14
Mean surface albedo walls	Assumption/literature	0.4
Canyon width, in meters	GIS	0–220
Height of walls, in meters	GIS	0–53
Orientation of street canyon wall	GIS	0–360
Heat storage coefficients (ground & walls)	OHM model (Grimmond & Oke, 2002)	Ground (A1): 0.61 Ground (A2): 0.41 Ground (A3): -28.0 Wall 1,2 (A1): 0.83 Wall 1,2 (A2): 0.43 Wall 1,2 (A3): -54.0
Mixing ratio for atmos. conditions	Erell et al., 2009; 2010	Inversion: 0.894 Stable: 0.935 Neutral: 0.948 Turbulent: 0.973 Super stable: 0.809
LUMPS Beta value	Erell & Williamson, 2006	5
Plant and water cover (%)	GIS/Remote sensing	1–1

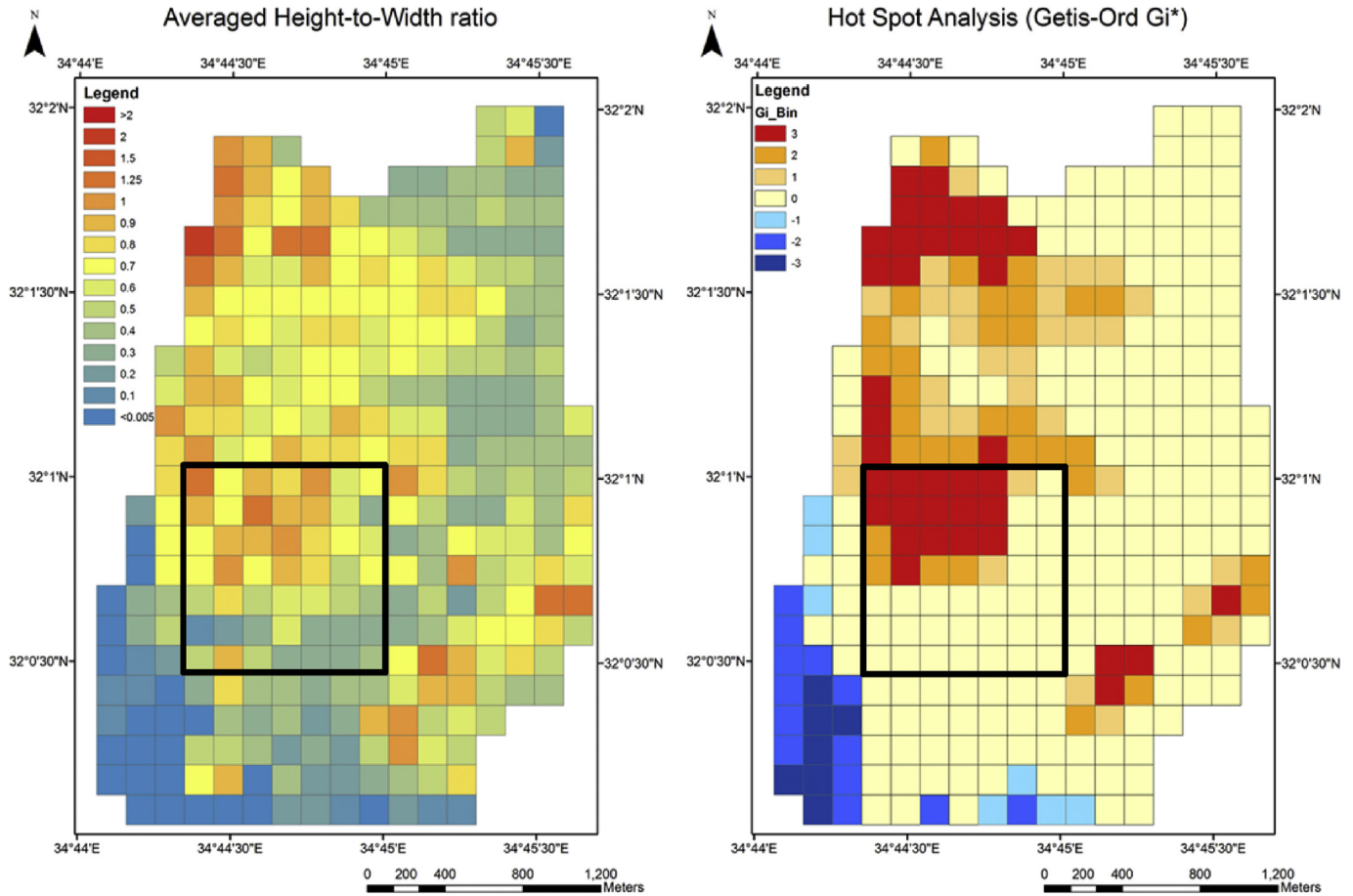


Fig. 4. The spatial pattern of H/W (left) and hot-spot analysis (right). The black square represents the 7×7 matrix used to run CAT.

2.4.2.2. Building height. The building footprint layer includes the height for each building. To assign the mean height for a street a new raster was generated, where the value of each pixel is the height of the building closest to it. For convenience and accuracy we used a grid size of 1×1 m. We then repeated the procedure elaborated above using the Zonal Statistics and the streets buffer, and assigned to each street segment the mean value of the buildings heights within its buffer. In addition to canyon geometry, we also computed the street orientation (azimuth).

The radiative and conductive properties of building materials also affect heating/cooling (Grimmond, 2007). Such data are not available in many cities, and field work at such a scale is not feasible. Thus, the radiative and conductive properties were estimated from previous work and the literature, and assumed to be constant throughout the city.

2.4.3. Albedo

Ground albedo is a key forcing parameter on the surface energy balance and hence the UHI, so it is important to account for its spatial variability, especially in urban areas where surface land cover varies greatly over short distances. Since CAT requires independent values of the ground albedo for each 150 m grid cell, the buildings footprint was masked and the average albedo was estimated using the empirical formula previously developed for the Landsat TM/ETM+ sensor (Liang, 2000):

$$\alpha_{vis} = 0.443b_2 + 0.317b_3 + 0.240b_5$$

where b_2 , b_3 , b_5 correspond to the reflectance in WV2 spectral

bands 2 (0.45–0.51 μm), 3 (0.51–0.58 μm) and 5 (0.63–0.69 μm), respectively.

The average albedo values of the ground surface of the 150 m grid cells in the test area range from 0.08 to 0.14, although individual pixels varied from 0.02 to 0.34. Table 1 summarizes the CAT inputs describing an urban site, and the methods used to estimate them.

CAT input also includes albedo of each of the walls comprising the street canyon. Because this cannot be estimated by remote sensing, the value for wall albedo was assessed manually. A visit to the study area and visual analysis of Google Earth images show most walls are of rough, off-white/beige plaster, so in the absence of more detailed data, a fixed value of albedo = 0.4 was used. The ground surface near the meteorological site is mostly bare soil and was assigned a fixed albedo of 0.3.

2.4.4. Urban canyon vs. open space

In CAT, the heat storage coefficients values are described by the objective hysteresis model (OHM) by Grimmond and Oke (2002). These coefficients are different for an urban canyon and for an open space within the city. To determine whether a grid cell is an urban canyon or an open space and assign correct values from the OHM, the land cover frequency within each 150 m grid cell was calculated using the zonal statistics tool in ArcGIS (ESRI, 1984). Because CAT focuses on canyon 3D geometry, and following the USA National Land Cover Data (NLCD) guidelines (Homer et al., 2015), each grid cell with a built fraction <0.2 was classified as open space. Open space grid cells, which CAT models as very shallow street canyons,

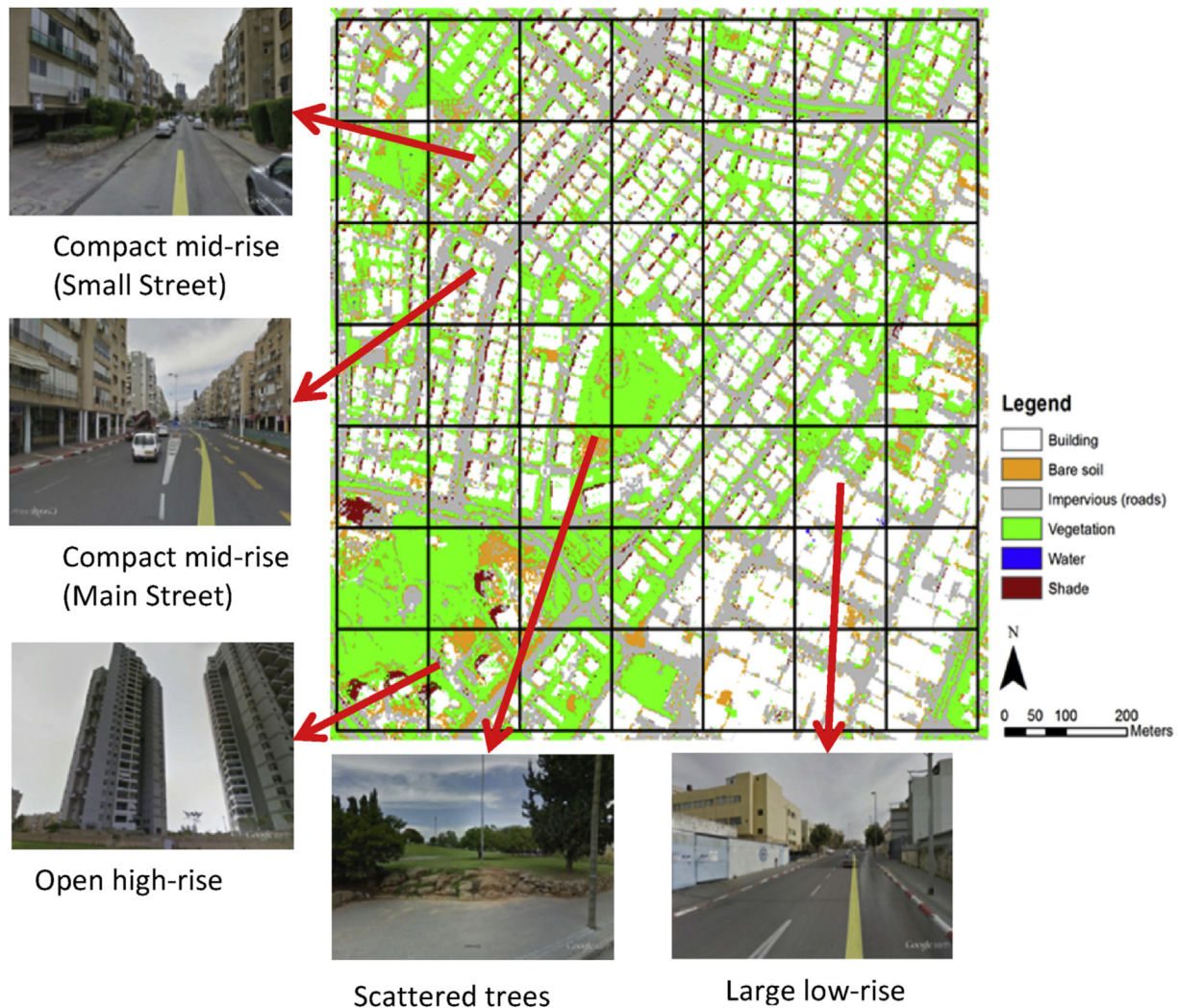


Fig. 5. Land cover classification and typical types of street morphology based on the local climate zones classification (Stewart & Oke, 2012).

were assigned a 'building' height of 3 m and 'canyon' width of 150 m, corresponding to a sky view factor of approximately 0.99. We assume that even in an open space there are some features such as topography, trees and possibly some man made features; thus the sky view factor is not 1.0.

3. Results

3.1. Urban 3D geometry

Fig. 4 shows the spatial pattern of H/W for the study area and its subsequent hot/cold cluster analysis using the Getis-Ord G_i^* statistic (Getis & Ord, 1996; Ord & Getis, 1995). The G_i^* statistic is a method for analyzing spatial clustering in data by identifying statistically significant hot and cold spots. Positive values of G_i^* indicate a cluster of high data values, while negative values of G_i^* indicate a cluster of low data values. The degree of clustering and its statistical significance is represented using the G_i bin output in Fig. 4. Features in the ± 3 bins represent statistical significance with a 99% confidence level; features in the ± 2 bins represent a 95% confidence level; features in the ± 1 bins represent a 90% confidence level; and the clustering for features in bin 0 is not statistically significant. Results indicate that the city average H/W ratio is approximately 0.5, ranging from 0 to 1.96. Higher H/W is observed

on the north-west of the city, where the main land use is small residential and retail buildings 3–5 stories tall. The lower H/W values correspond to open spaces and residential buildings 1–3 stories tall; the higher values on the south-east corner of the city correspond to the city's light-industry area. These results demonstrate the methodology's ability to capture the spatial variability of Bat-Yam's urban geometry.

The cluster analysis (Fig. 4, right) used to identify areas that potentially lead to more intense UHIs suggests that two main hot-spots exist, i.e. – a grid cell with high H/W surrounded by other grid cells with high H/W values. The cold cluster corresponds to the beach strip and open space (see Fig. 1). To provide a proof of concept for our methodology and demonstrate the importance of the fine scale spatial variability of the urban morphology, a sub-sample of the whole city that maximizes spatial variability was selected for further analysis (Fig. 4). The sub-sample, comprising a 7×7 matrix, was chosen because it includes a wide range of H/W ratio as well as a hot-spot of H/W where we expect a larger UHI to form.

3.2. Land cover and local climate zones

Fig. 5 shows the land cover map and the typical streets for the 7×7 sample area, classified according to the local climate zones

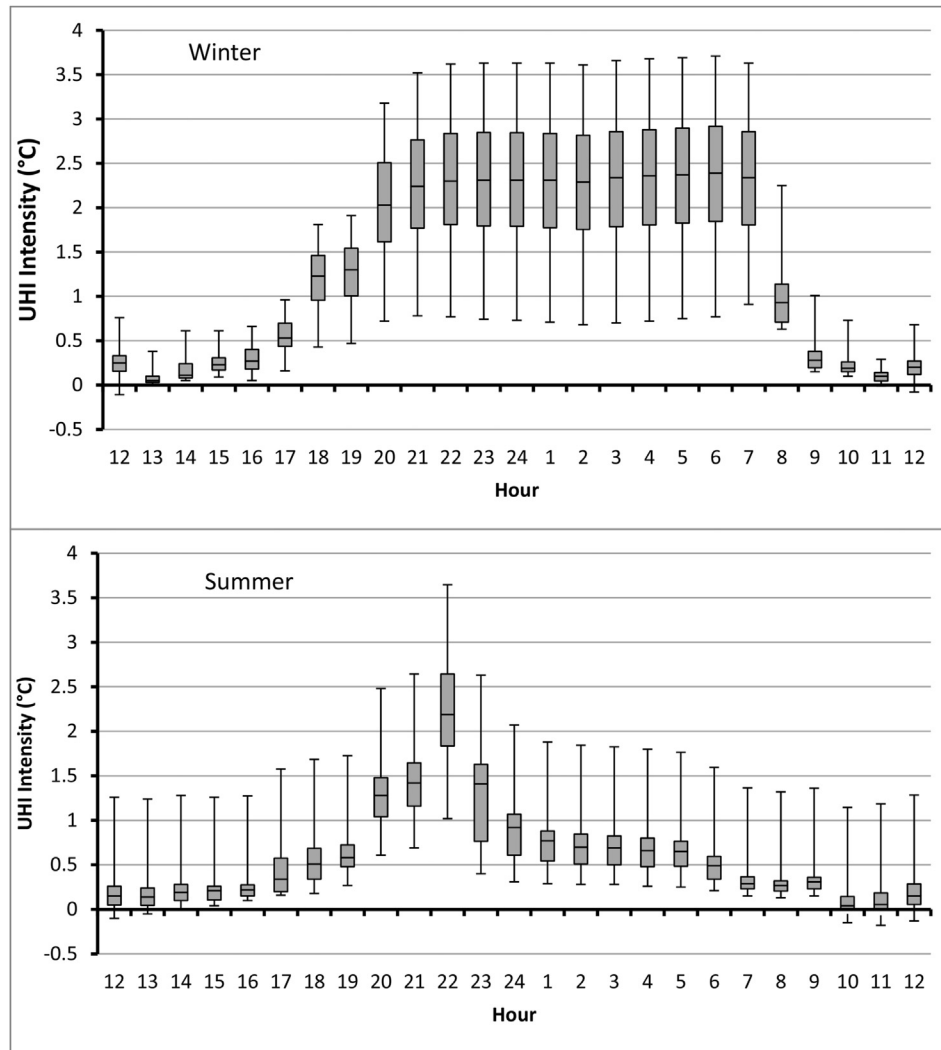


Fig. 6. Hourly UHI intensity and variability across all 49 grid-cells for January 15–16 (top) and August 15–16 (bottom). The gray box represents the second and third quartiles and the horizontal black line represents the median. Whiskers indicate highs and lows for each hour.

developed by [Stewart and Oke \(2012\)](#). The area's surface cover consists of 26% buildings, 21% impervious (roads) and 52% pervious (19% bare soil and 33% vegetation). The scarcity of long-term data on local climate spatial variability within cities ([van Hove et al., 2015](#)) and the existence of multiple local climate zones at this small scale further demonstrates the importance of predicting the spatial variability of the UHI within the city.

3.3. Urban heat island

The urban-rural temperature difference (ΔT_{u-r}) was simulated by CAT for each grid-cell. The model was run for all grid-cells simultaneously, using each cell's unique parameters as extracted from the GIS and remote sensing data (see [Table 1](#)). [Fig. 6](#) shows the diurnal development of ΔT_{u-r} across all 49 grid cells for a clear day in winter and summer. In winter, a distinct UHI is observed at night time, with a lower intensity during daytime. During nighttime hours urban-rural temperature differences increase, as does the spatial variability between grid cells: From 20:00 LST to 07:00 LST the next day, a stable UHI is observed, ranging from 0.75 °C for open urban spaces to over 3.5 °C for grid cells with high H/W (compact mid-rise residential). Overall, for the winter day chosen, the UHI

displays the expected pattern, and reflects low air temperatures at the rural weather station at night (dry bulb temperature ranges 3–8 °C between Jan 15, 22:00 and Jan 16, 08:00).

During daytime, urban-rural temperature differences are much lower, with a mean intensity of less than 0.5 °C. Intra-urban variability is much smaller and ΔT_{u-r} has a distinct positive skewness, with a small number of cells displaying a substantial temperature difference while most others were characterized by a much more modest one. This is even more obvious in summer-time where during the entire diurnal cycle a positive skewness is observed.

On average, considering all grid cells, a maximum average temperature difference of ~2.35 °C was observed in both seasons. Similar temperature differences were reported by [Saaroni et al. \(2000\)](#) for the neighboring city of Tel-Aviv. Following [Kaplan, Georgescu, Alfasi, and Kloog \(2015\)](#), the relative day-time cooling (or, damping of warming expected with urban expansion) was attributed to changes in energy partitioning. In summer, early evening hours are characterized by little or no wind, allowing the UHI to develop until it peaks at 22:00 LST. [Goldreich \(1982\)](#) found a similar temporal pattern for Tel-Aviv. After 22:00 the wind picks up again as the land breeze starts, acting as a cooling agent ([Heisler,](#)

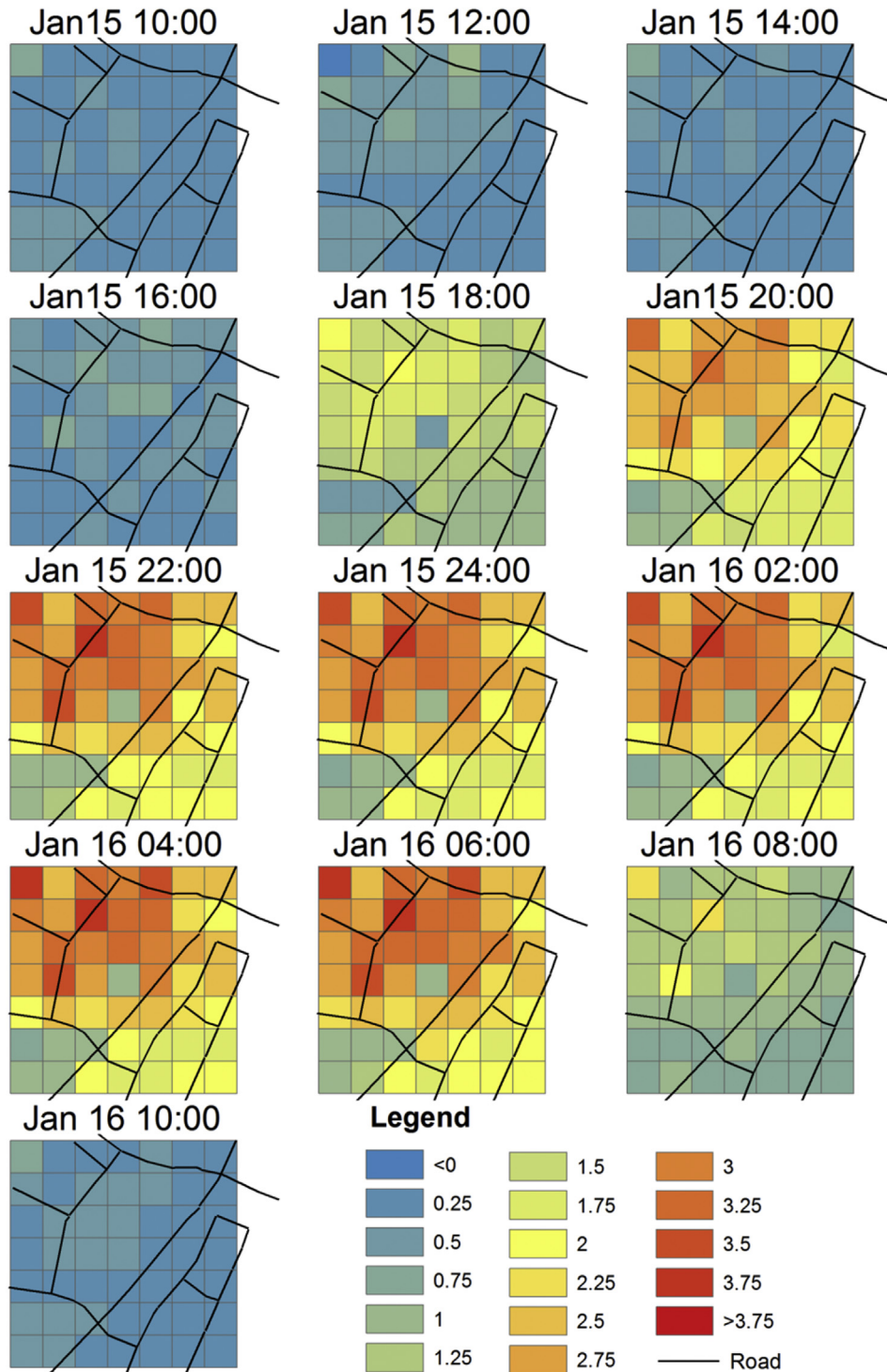


Fig. 7. Spatial and temporal development of the temperature field (°C) on a winter day (Jan 15, 10am to Jan 16, 10am).

Ellis, Nowak, & Yesilonis, 2015; Saaroni et al., 2000), causing the UHI to dissipate rapidly.

One of the advantages of coupling CAT with GIS is the ability to represent and visualize the results to include the spatial domain and highlight both the spatial variability and the effect of the different H/W of each grid cell. Fig. 7 shows maps of the spatio-temporal development ΔT_{u-r} at two-hour intervals for a typical clear-sky winter day. Similarly, Fig. 8 shows the same for summer

[See supplementary materials for animated versions of these figures]. In both winter and summer the UHI intensity reflects the street canyon aspect ratio, as illustrated in Fig. 4. In winter, a maximum nighttime UHI of up to 3.75 °C is predicted in the dense residential areas (see Fig. 5 for location of the different land use types). The low- and mid-rise area (light industry) shows a lower ΔT_{u-r} of up to 2.45 °C. At peak intensity (22:00–23:00), the minimum predicted ΔT_{u-r} is 0.77 °C at the open space/park in the south

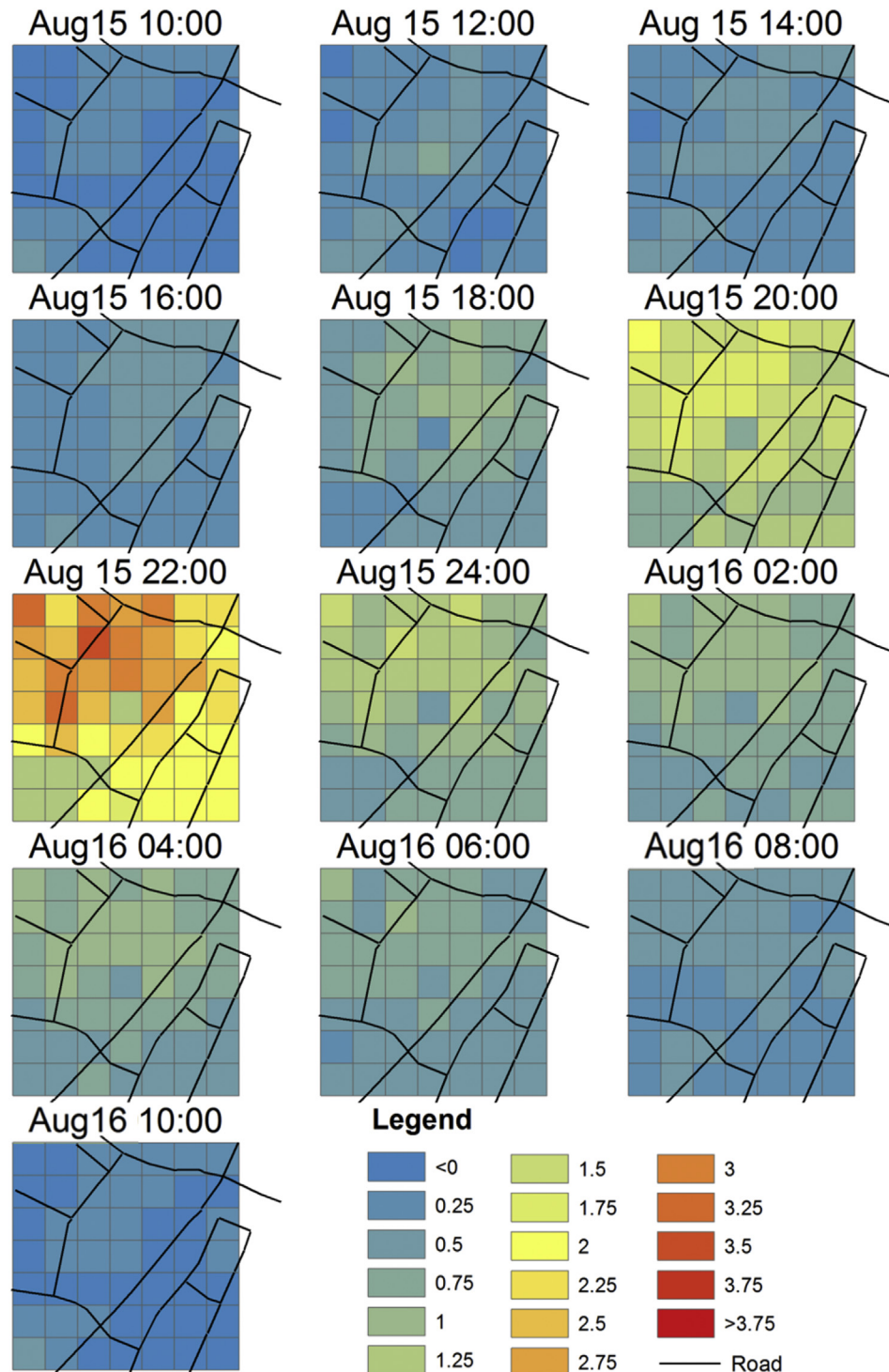


Fig. 8. Spatial and temporal development of the temperature field (°C) on a summer day (Aug 15, 10am to Aug 16, 10am).

west corner of the domain. These results are in line with [van Hove et al. \(2015\)](#) and [Ivajnsić et al. \(2014\)](#) who found that intra-urban variability in air temperature is significantly related to land cover fractions and mean building height. The lowest temperature within the city is observed in the park at the center of our domain with $\Delta T_{u-r} = 0.86$, similar to [Shashua-Bar and Hoffman \(2000\)](#) who showed that urban parks may have a cooling effect of 1.5 °C–3 °C compared to the adjacent built environment.

From [Fig. 7](#) we note that during winter all grid cells, including

open space, show a relative temperature elevation in comparison with the reference site throughout the night. In summer ([Fig. 8](#)), the simulation predicts less spatial variability with a maximum temperature elevation of 3.3 °C. [Saaroni et al. \(2000\)](#) reported similar UHI values for Tel-Aviv, where the UHI intensity can reach up to 6 °C during nighttime. It is important to note that the same grid-cell shows maximum temperature anomalies for both summer and winter. This grid cell is classified as 'residential mid-rise' with $H/W = 1.08$, and is located in the center of the hot-spot cluster, i.e.

surrounded by other grid cells which also have relatively high values of the canyon aspect ratio. For both times of year, daytime hours show no significant temperature anomalies.

4. Discussion

Current top-down methods are susceptible to an inherent error due to the inability to represent the full spatial variability of local, small-scale surface characteristics and canyon geometry (which are therefore typically represented by a mean or parameterization scheme); In contrast, the approach proposed here provides a detailed representation of the variability of the surface cover and spatial geometry. The number of locations that can be modeled is not limited and therefore can provide a more accurate representation of the spatial micro-climatic variations. This comes at a cost, however, due to the simplifying assumption in CAT of a horizontally homogenous boundary layer above the reference site and the urban area being studied. The method can therefore be applied only where there are no overriding mesoscale phenomena, such as the effect of large variations in topography, which might drown the urban signal.

One limitation of our grid based approach is that it assigns each grid average 3D values. This can be overcome to some extent by increasing the spatial resolution, i.e. – using a smaller grid cell size. Although this increases the computation cost of the model, the primary limitation is actually the size of the urban elements that comprise the study area. Each grid cell must, for example, encompass at least the width of the buildings and the street canyon they define, as well as a canyon length that is sufficiently long so that end effects may be ignored.

In addition, using a grid approach introduces an inherent problem of the location of the origin. If the size of the grid cell is sufficiently small, then the origin point of the grid should be of no importance. However, minor inconsistencies may result if, for example, a small park is completely represented by one grid cell or divided among two adjacent cells that are primarily built-up.

The visualization of urban temperature variability is an important benefit for decision makers and urban planners. Coupling the CAT model with GIS enables us to generate snapshots illustrating the urban influence on the spatio-temporal variability of air temperature, as well as to generate 'urbanized' TMYs. The latter can be utilized for building simulation purposes, as well as for urban planning requiring evaluation and comparison of different scenarios (such as location, size and distribution of green open spaces). Incorporating climatological information in city design can provide a better living and working environment for inhabitants (Georgescu, Morefield, Bierwagen, & Weaver, 2014; Kaplan et al., 2015; Roth, 2007). By using the bottom-up approach, we demonstrated that it is relatively easy to generate a climate map that can be easily interpreted by planners and/or other stakeholders. In general, the methodology presented here to extract 3D parameters can be used with other micro- and meso-scale climate models that require an input of the street geometry and land cover.

5. Conclusion and implications for urban planning

The changing face of cities that often accompanies rapid urbanization and the potential impact of climate change pose challenges that urban planners must overcome. Tools are required to assess the effect of increased spatial variability of land use and land cover, and the effect of mitigation/adaptation measures to reduce the effects of the UHI (van Hove et al., 2015) in different scenarios. We have demonstrated how GIS-based, spatially distributed urban canyon 3D geometry and land cover information obtained from remote sensing can be linked with an urban canyon model to

generate a detailed map of the spatial and temporal intra-urban variability of air temperatures. Applying the model for the city of Bat-Yam, Israel, a mean nighttime UHI of 2 °C–2.25 °C was predicted during both summer and winter, with significant spatial variability attributed to differences in the height-to-width ratio and the variability of land use and surface cover. The CAT computer simulation also illustrated the importance of the local wind regime on the nocturnal UHI.

We conclude that the application of the CAT model supports simulations at the city scale that reflect intra-urban variability. Identification of the spatio-temporal variability of the UHI in a city can lead to a better understanding of its causes as well as its implications for thermal stress and to plan appropriate geographically specific mitigation and adaptation measures. These may have further relevance for environmental implications in a time of global warming, especially in a warm region such as the Mediterranean basin.

Supplementary video related to this article can be found at <http://dx.doi.org/10.1016/j.apgeog.2016.09.015>.

Acknowledgments

This research was made possible with the support of the Jewish National Fund. Shai Kaplan was also supported by the Jacob Blaustein Center for Scientific Cooperation. The authors would also like to thank Mr. Kobi Nahon for creating the animations.

References

- Arnfield, A. J. (2003). Two decades of urban climate research: A review of turbulence, exchange of energy and water, and the urban heat island. *International Journal of Climatology*, 23(1), 1–26.
- Basu, R., & Samet, J. M. (2002). Relation between elevated ambient temperature and mortality: A review of the epidemiologic evidence. *Epidemiologic Reviews*, 24, 190–202. <http://dx.doi.org/10.1093/epirev/mxf007>.
- Bitan, A., & Rubin, S. (1994). *Climatic atlas of Israel for physical and environmental planning and design*. Tel Aviv, Israel: Ramot Publishing Company, Tel-Aviv University.
- Bruse, M., & Fleer, H. (1998). Simulating surface–plant–air interactions inside urban environments with a three dimensional numerical model. *Environmental Modelling & Software*, 13(3–4), 373–384. [http://dx.doi.org/10.1016/S1364-8152\(98\)00042-5](http://dx.doi.org/10.1016/S1364-8152(98)00042-5).
- Chow, W. T. L., & Roth, M. (2006). Temporal dynamics of the urban heat island in Singapore. *International Journal of Climatology*, 26, 2243–2260. <http://dx.doi.org/10.1002/joc.1364>.
- Erell, E., Eliasson, I., Grimmond, S., Offerle, B., & Williamson, T. (2009). Incorporating spatial and temporal variations of advected moisture in the canyon air temperature (Cat) model. In *The seventh international conference on urban climate, (January 2016)*.
- Erell, E., Eliasson, I., Grimmond, S., Offerle, B., & Williamson, T. (2010). The effect of stability on estimated variations of advected moisture in the canyon air temperature (CAT) model. In *The 9th AMS symposium on the urban environment (Vol. 1, pp. 3–8)*.
- Erell, E., & Williamson, T. (2006). Simulating air temperature in an urban street canyon in all weather conditions using measured data at a reference meteorological station. *International Journal of Climatology*, 26(12), 1671–1694. <http://dx.doi.org/10.1002/joc>.
- Erell, E., & Williamson, T. (2007). Intra-urban differences in canopy layer air temperature at a mid-latitude city. *International Journal of Climatology*, 27(9), 1243–1255. <http://dx.doi.org/10.1002/joc.1469>.
- ESRI. (1984). *ArcGIS desktop 10.3. Redlands*.
- Georgescu, M., Morefield, P. E., Bierwagen, B. G., & Weaver, C. P. (2014). Urban adaptation can roll back warming of emerging megapolitan regions. *Proceedings of the National Academy of Sciences of the United States of America*, 111(8), 2909–2914. <http://dx.doi.org/10.1073/pnas.1322280111>.
- Georgescu, M., Moustauoui, M., Mahalov, A., & Dudhia, J. (2012). Summer-time climate impacts of projected megapolitan expansion in Arizona. *Nature Climate Change*, 3(1), 37–41. <http://dx.doi.org/10.1038/nclimate1656>.
- Getis, A., & Ord, J. K. (1996). Local spatial statistics: An overview. In P. Longley, & M. Batty (Eds.), *Spatial analysis: Modelling in a GIS environment* (pp. 261–278). New York, USA: John Wiley & Sons, Inc.
- Giridharan, R., Ganesan, S., & Lau, S. S. Y. (2004). Daytime urban heat island effect in high-rise and high-density residential developments in Hong Kong. *Energy and Buildings*, 36, 525–534. <http://dx.doi.org/10.1016/j.enbuild.2003.12.016>.
- Giridharan, R., Lau, S. S. Y., & Ganesan, S. (2005). Nocturnal heat island effect in urban residential developments of Hong Kong. *Energy and Buildings*, 37,

- 964–971. <http://dx.doi.org/10.1016/j.enbuild.2004.12.005>.
- Goldreich, Y. (1982). Urban climate aspects in the greater Tel Aviv. In D. Grossman (Ed.), *Between Yarkon and Ayyalon* (pp. 12–22). Ramat Gan: Bar Ilan Publ.
- Grimmond, C. S. B. (2007). *Urbanization and global environmental change: Local effects of urban warming* (Vol. 173(1), pp. 83–88).
- Grimmond, C. S. B., & Oke, T. R. (2002). Turbulent heat fluxes in urban Areas: Observations and a local-scale urban meteorological parameterization scheme (LUMPS). *Journal of Applied Meteorology*, 41(7), 792–810. [http://dx.doi.org/10.1175/1520-0450\(2002\)041<0792:THFUA>2.0.CO;2](http://dx.doi.org/10.1175/1520-0450(2002)041<0792:THFUA>2.0.CO;2).
- Guo, Y., Gasparrini, A., Armstrong, B., Li, S., Tawatsupa, B., Tobias, A., et al. (2014). Global variation in the effects of ambient temperature on mortality: A systematic evaluation. *Epidemiology*, 25(6), 781–789. <http://dx.doi.org/10.1097/EDE.0000000000000165>.
- Hamdi, R., & Masson, V. (2008). Inclusion of a drag approach in the Town energy balance (TEB) Scheme: Offline 1D evaluation in a street canyon. *Journal of Applied Meteorology and Climatology*, 47(10), 2627–2644. <http://dx.doi.org/10.1175/2008JAMC1865.1>.
- Hart, M. A., & Sailor, D. J. (2009). Quantifying the influence of land-use and surface characteristics on spatial variability in the urban heat island. *Theoretical and Applied Climatology*, 95, 397–406. <http://dx.doi.org/10.1007/s00704-008-0017-5>.
- Heisler, G. M., Ellis, A., Nowak, D. J., & Yesilonis, I. (2015). Modeling and imaging land-cover influences on air temperature in and near Baltimore, MD. *Theoretical and Applied Climatology*. <http://dx.doi.org/10.1007/s00704-015-1416-z>.
- Homer, C. G., Dewitz, J. A., Yang, L., Jin, S., Danielson, P., Xian, G., et al. (2015). Completion of the 2011 National land cover database for the coterminous United States - Representing a decade of land cover change information. *PE&RS*, 81(5), 345–354. Retrieved from http://www.asprs.org/a/publications/pers/2015journals/PERS_May_2015/HTML/index.html#345/z.
- Howard, L. (1820). *Climate of London*.
- van Hove, L. W. A., Jacobs, C. M. J., Heusinkveld, B. G., Elbers, J. A., van Driel, B. L., & Holtslag, A. A. M. (2015). Temporal and spatial variability of urban heat island and thermal comfort within the Rotterdam agglomeration. *Building and Environment*, 83, 91–103. <http://dx.doi.org/10.1016/j.buildenv.2014.08.029>.
- Ivajnsic, D., Kaligarić, M., & Žiberna, I. (2014). Geographically weighted regression of the urban heat island of a small city. *Applied Geography* (Vol. 53., 341–353).
- Jusuf, S. K., & Hien, W. N. (2009). Development of empirical models for an estate level air temperature prediction in Singapore. In *Proceedings of the second international conference on countermeasures to urban heat islands, Berkeley, California, Sept 21-23*.
- Kaplan, S., Georgescu, M., Alfasi, N., & Kloog, I. (2015). Impact of future urbanization on a hot summer: A case study of Israel. *Theoretical and Applied Climatology*. <http://dx.doi.org/10.1007/s00704-015-1708-3>.
- Kastendeuch, P., & Najjar, G. (2015). Simulation of urban fluxes with a 3D canopy model. In *ICUC9-9th international conference on urban climate, Toulouse, France*.
- Kloog, I., Chudnovsky, A., Koutrakis, P., & Schwartz, J. (2012). Temporal and spatial assessments of minimum air temperature using satellite surface temperature measurements in Massachusetts, USA. *The Science of the Total Environment*, 432, 85–92. <http://dx.doi.org/10.1016/j.scitotenv.2012.05.095>.
- Kloog, I., Nordio, F., Coull, B. A., & Schwartz, J. (2014). Predicting spatiotemporal mean air temperature using MODIS satellite surface temperature measurements across the Northeastern USA. *Remote Sensing of Environment*, 150, 132–139. <http://dx.doi.org/10.1016/j.rse.2014.04.024>.
- Laaidi, K., Zeghnoun, A., Dousset, B., Bretin, P., Vandentorren, S., Giraudet, E., et al. (2012). The impact of heat islands on mortality in Paris during the August 2003 heat wave. *Environmental Health Perspectives*, 120(2), 254–259. <http://dx.doi.org/10.1289/ehp.1103532>.
- Liang, S. (2000). *Narrowband to broadband conversions of land surface albedo I Algorithms*. Retrieved February 7, 2016, from http://ac.els-cdn.com/S0034425700002054/1-s2.0-S0034425700002054-main.pdf?_tid=bf6e12c6-cd67-11e5-8ce4-0000aacb35d&acdnat=1454828298_f41902877e1ffa96d3df5b4e652025c9.
- Lillesand, T. M., Kiefer, R. W., & Chipman, J. W. (2007). *Remote sensing and image interpretation* (6th ed.).
- Lloyd, C. D. (2010). *Spatial data analysis*. New York: Oxford University Press Inc.
- Lookingbill, T. (2003). Spatial estimation of air temperature differences for landscape-scale studies in montane environments. *Agricultural and Forest Meteorology*, 114(3–4), 141–151. [http://dx.doi.org/10.1016/S0168-1923\(02\)00196-X](http://dx.doi.org/10.1016/S0168-1923(02)00196-X).
- Loridan, T., & Grimmond, C. S. B. (2012). Multi-site evaluation of an urban land-surface model: Intra-urban heterogeneity, seasonality and parameter complexity requirements. *Quarterly Journal of the Royal Meteorological Society*, 138(665), 1094–1113. <http://dx.doi.org/10.1002/qj.963>.
- Masson, V. (2000). A physically-based scheme for the urban energy budget in atmospheric models. *Boundary-Layer Meteorology*, 94(3), 357–397. <http://dx.doi.org/10.1023/A:1002463829265>.
- Merbitz, H., Buttstädt, M., Michael, S., Dott, W., & Schneider, C. (2012). GIS-based identification of spatial variables enhancing heat and poor air quality in urban areas. *Applied Geography*, 33, 94–106. <http://dx.doi.org/10.1016/j.apgeog.2011.06.008>.
- Mizuno, M., Nakamura, Y., Murakami, H., & Yamamoto, S. (1990). Effects of land use on urban horizontal atmospheric temperature distributions. *Energy and Buildings*, 15(1–2), 165–176. [http://dx.doi.org/10.1016/0378-7788\(90\)90128-6](http://dx.doi.org/10.1016/0378-7788(90)90128-6).
- Oke, T. R. (1973). City size and the urban heat island. *Atmospheric Environment* (1967), 7(8), 769–779. [http://dx.doi.org/10.1016/0004-6981\(73\)90140-6](http://dx.doi.org/10.1016/0004-6981(73)90140-6).
- Oke, T. R. (1981). Canyon geometry and the nocturnal urban heat island: Comparison of scale model and field observations. *Journal of Climatology*, 1(3), 237–254. <http://dx.doi.org/10.1002/joc.3370010304>.
- Oke, T. R. (1982). The energetic basis of the urban heat island. *Quarterly Journal of the Royal Meteorological Society*, 108(455), 1–24. <http://dx.doi.org/10.1002/qj.49710845502>.
- Oke, T. R. (1987). *Boundary layer climates*. Retrieved from <https://books.google.com/books?hl=iw&lr=&id=RVyIAgAAQBAJ&pgis=1>.
- Oleson, K. W., Bonan, G. B., Feddema, J., Vertenstein, M., & Grimmond, C. S. B. (2008). An urban parameterization for a global climate model. Part I: Formulation and evaluation for two cities. *Journal of Applied Meteorology and Climatology*, 47(4), 1038–1060. <http://dx.doi.org/10.1175/2007JAMC1597.1>.
- Ord, J. K., & Getis, A. (1995). Local spatial autocorrelation Statistics: Distributional issues and an application. *Geographical Analysis*, 27(4), 286–306. <http://dx.doi.org/10.1111/j.1538-4632.1995.tb00912.x>.
- Pelta, R., Chudnovsky, A. A., & Schwartz, J. (2016). Spatio-temporal behavior of brightness temperature in Tel-Aviv and its application to air temperature monitoring. *Environmental Pollution (Barking, Essex: 1987)*, 208(Pt A), 153–160. <http://dx.doi.org/10.1016/j.envpol.2015.09.007>.
- Pielke, R. A. (2001). Influence of the spatial distribution of vegetation and soils on the prediction of cumulus Convective rainfall. *Reviews of Geophysics*, 39(2), 151. <http://dx.doi.org/10.1029/1999RG000072>.
- Ren, C., Ng, E. Y., & Katschner, L. (2011). Urban climatic map studies: A review. *International Journal of Climatology*, 31(15), 2213–2233. <http://dx.doi.org/10.1002/joc.2237>.
- Robine, J., Cheung, S. L. K., Le Roy, S., Van Oyen, H., Griffiths, C., Michel, J., et al. (2008). Death toll exceeded 70,000 in Europe during the summer of 2003. *Comptes Rendus Biologies*, 331, 171–178. <http://dx.doi.org/10.1016/j.crvi.2007.12.001>.
- Rosenthal, J., Kinney, P., & Metzger, K. (2014). Intra-urban vulnerability to heat-related mortality in New York City, 1997–2006. *Health and Place*, 30, 45–60. <http://dx.doi.org/10.1016/j.healthplace.2014.07.014>.
- Rotem-Mindali, O., Michael, Y., Helman, D., & Lensky, I. M. (2015). The role of local land-use on the urban heat island effect of Tel Aviv as assessed from satellite remote sensing. *Applied Geography*, 56, 145–153. <http://dx.doi.org/10.1016/j.apgeog.2014.11.023>.
- Roth, M. (2007). Review of urban climate research in (sub)tropical regions. *International Journal of Climatology*, 27(14), 1859–1873. <http://dx.doi.org/10.1002/joc.1591>.
- Saaroni, H., Ben-Dor, E., Bitan, A., & Potchter, O. (2000). Spatial distribution and microscale characteristics of the urban heat island in Tel-Aviv, Israel. *Landscape and Urban Planning*, 48, 1–18. [http://dx.doi.org/10.1016/S0169-2046\(99\)00018-3](http://dx.doi.org/10.1016/S0169-2046(99)00018-3).
- Schmid, H. P., & Oke, T. R. (1990). A model to estimate the source area contributing to turbulent exchange in the surface layer over patchy terrain. *Quarterly Journal of the Royal Meteorological Society*, 116, 965–988. <http://dx.doi.org/10.1002/qj.49711649409>.
- Shashua-Bar, L., & Hoffman, M. E. (2000). Vegetation as a climatic component in the design of an urban street. *Energy and Buildings*, 31(3), 221–235. [http://dx.doi.org/10.1016/S0378-7788\(99\)00018-3](http://dx.doi.org/10.1016/S0378-7788(99)00018-3).
- Stewart, I. D., & Oke, T. R. (2012). Local climate zones for urban temperature studies. *Bulletin of the American Meteorological Society*, 93(12), 1879–1900. <http://dx.doi.org/10.1175/BAMS-D-11-00019.1>.
- Weaver, C. P., & Avissar, R. (2001). Atmospheric disturbances caused by human modification of the landscape. *Bulletin of the American Meteorological Society*, 82(2), 269–281. [http://dx.doi.org/10.1175/1520-0477\(2001\)082<0269:ADCBHM>2.3.CO;2](http://dx.doi.org/10.1175/1520-0477(2001)082<0269:ADCBHM>2.3.CO;2).
- Williamson, T. J. (1995). A confirmation technique for thermal performance simulation models. *Building performance. Building Simulation*, 268–275 (Madison, WI).
- Yang, Y., Endreny, T. A., & Nowak, D. J. (2013). A physically based analytical spatial air temperature and humidity model. *Journal of Geophysical Research: Atmospheres*, 118(18), 10,449–10,463. <http://dx.doi.org/10.1002/jgrd.50803>.